Coastal Engineering 117 (2016) 191–204

Contents lists available at ScienceDirect

Coastal Engineering

journal homepage: www.elsevier.com/locate/coastaleng

Estimation of time-varying discharge and cumulative volume in individual overtopping waves

Steven A. Hughes [a,*], Christopher I. Thornton [b]

[a] Engineering Research Center, Department of Civil and Environmental Engineering, 1320 Campus Delivery, Colorado State University, Fort Collins, CO 80523-1320, United States
[b] Engineering Research Center, Department of Civil and Environmental Engineering, 1320 Campus Delivery, Colorado State University, Fort Collins, CO 80523-1320, United States

ARTICLE INFO

Article history:
Received 22 March 2016
Received in revised form 3 August 2016
Accepted 15 August 2016
Available online 2 September 2016

Keywords:
Wave overtopping
Time-varying discharge
Cumulative overtopping volume
Weibull equation
Individual overtopping wave parameters

ABSTRACT

The time variation of discharge per unit dike length in an overtopping wave is characterized by a rapid increase to a maximum discharge that can be several times greater than the mean discharge, followed by a slower decrease in discharge until overtopping for that wave ceases. Measurements of wave overtopping acquired during the European small-scale *FlowDike* experiments were analyzed to identify individual overtopping waves using a two-step "supervised" procedure that combines the best features of automated wave determination augmented with manual error correction and validation. The result was a well-vetted data set of 5799 individual overtopping waves represented by time-series of flow depth and velocity near the seaward edge of the dike crest. The model dikes had planar seaward dike slopes of either 1V-on-3H or 1V-on-6H. Instantaneous discharge time series were calculated as the product of the flow thickness and velocity time series. In this paper, the two-parameter Weibull probability density function is adopted to represent the time variation of instantaneous discharge in an overtopping wave. Values of the Weibull scale factors, a, and shape factors, b, are obtained through nonlinear best-fitting of the Weibull equation to all 5799 waves. Best fits were also performed for the simpler Rayleigh version of the Weibull equation when $b = 2$. An empirical equation was developed for scale factor, a, in terms of predicable parameters of the overtopping waves. The shape factor, b, could not be successfully parameterized, but it was found that the shape factors are narrowly distributed about the Rayleigh value of $b = 2$. Predictions of time-varying discharge made using the Weibull equation with $b = 2$ (i.e., Rayleigh equation) are assessed in terms of the root-mean-square errors between predictions and measurements. The estimates are reasonable for most of the waves. The capability to estimate the time-varying discharge in individual overtopping waves will improve the art of full-scale wave overtopping simulation, and the resulting empirical equations will contribute to methodologies aimed at quantifying the resiliency of dike erosion protection.

1. Introduction

The capability of grass-covered earthen dikes and levees to withstand tolerable rates of wave overtopping depends almost entirely on the resiliency of the grass/soil system protecting the landward-side slope. The applied hydrodynamic forces occurring during wave overtopping vary greatly with maximum instantaneous velocities being as much as four times greater than the average flow velocity. Furthermore, each successive overtopping wave has different magnitudes of maximum velocity, maximum flow thickness, maximum discharge, and overtopping duration. The time variation of instantaneous discharge in individual overtopping waves typically features a fairly rapid increase in discharge to a maximum value, followed by a much slower decline in discharge down to zero. Thus, the hydrodynamic forces exerted on the structure crest and landward-side slope grass/soil system are unsteady and depend significantly on the time variation of instantaneous discharge that occurs with each overtopping wave.

Development of reliable design guidance for overtopping of grass-covered dike systems requires full-scale field measurements during storm events or full-scale physical model simulations of overtopping events. Acquiring field measurements during actual severe wave overtopping events is extraordinarily problematic, so coastal engineers have instead focused on full-scale wave overtopping simulation using mobile simulators on actual dikes (e.g., Van der Meer et al., 2006; Van der Meer, 2007; Van der Meer et al., 2008; Steendam et al., 2010) and fixed simulators using prepared grass test trays (e.g., Thornton et al., 2011; Van der Meer et al., 2011; Thornton et al., 2014).

Realistic wave overtopping simulations are driven by present understanding of the overtopping processes and being able to replicate these processes with a reasonable level of accuracy. When wave conditions and freeboard remain relatively constant, the overall wave overtopping condition can be represented by the average discharge (q_w) and the

* Corresponding author.
E-mail addresses: shughes2@engr.colostate.edu (S.A. Hughes), thornton@engr.colostate.edu (C.I. Thornton).

http://dx.doi.org/10.1016/j.coastaleng.2016.08.006
0378-3839/

probability distribution of individual overtopping wave volumes (P_V). Reliable empirical equations describing q_w and P_V in terms of incident wave conditions, structure geometry, and crest freeboard (Pullen et al., 2007) have been developed based on small- and large-scale physical model tests of common dike geometries. Full-scale physical model simulation of individual waves using the Dutch-invented simulator consists of the intermittent release onto the dike crest of prescribed water volumes in such a manner that key parameters of the unsteady flow (i.e., maximum velocity, maximum flow thickness, and release duration) are correctly reproduced for each water volume in the probability distribution. It may be possible to improve wave overtopping simulations by assuring the water release also approximates the actual time-varying discharge on the dike crest. This will lead to improved design guidance and better assessment of grass-covered dike and levee resiliency.

This paper utilizes a comprehensive set of wave overtopping measurements acquired during the European small-scale *FlowDike* experiments to: (1) identify individual overtopping waves; (2) analyze the time-varying discharge per unit dike length in each wave; and (3) establish viable empirical predictive equations for time-varying discharge and cumulative overtopping volume. Section 2 briefly overviews previous research related to individual overtopping waves. Section 3 summarizes the *FlowDike* experiments and describes the data analysis. A theoretical equation based on the two-parameter Weibull probability density function is proposed in Section 4 to represent the time variation of discharge and corresponding time variation in cumulative overtopping volume. The theoretical equation is fitted to measured discharge and cumulative volume time series in Section 5, and empirical relationships for the Weibull parameters are developed in Section 6. The new predictive equations are evaluated relative to measurements in Section 7, and application to a recent dike slope resiliency assessment methodology is illustrated in Section 8. A summary and conclusions are given in Section 9.

2. Previous research

Initial estimates of individual overtopping wave hydraulic parameters were reported in papers by Schüttrumpf et al. (2002); Van Gent (2002); Schüttrumpf and Van Gent (2003); Schüttrumpf and Oumeraci (2005), and Bosman et al. (2008). Relationships were given at the seaward edge of the dike crest for the flow depth ($h_{2\%}$) and flow velocity ($u_{2\%}$) exceeded by 2% of the incident waves. The equations at the seaward edge of the crest ($x_c = 0$) were given by

$$h_{2\%}(x_c = 0) = C_{A,h}\,(R_{u2\%} - R_c) \tag{1}$$

and

$$u_{2\%}(x_c = 0) = C_{A,u}\,\sqrt{g(R_{u2\%} - R_c)} \tag{2}$$

where $R_{u2\%}$ is the vertical run-up elevation exceeded by 2% of the incident waves; R_c is the freeboard (dike crest elevation minus still water elevation); g is gravitational acceleration; and $C_{A,h}$ and $C_{A,u}$ are empirical coefficients. It was necessary to assume $h_{2\%}$ and $u_{2\%}$ are Rayleigh-distributed to estimate values at other percent exceedance.

Van der Meer et al. (2010) measured flow thickness and velocity of eight different wave volume releases from the Dutch mobile overtopping simulator on an actual dike, and they developed relationships for maximum flow thickness, maximum velocity, and overtopping duration in terms of individual wave volume. Van der Meer et al. stated that the resulting equations were strictly valid only for the Dutch mobile simulator. They also recommended additional research to better resolve the dependency of the important wave volume parameters on individual wave volumes, and they questioned the assumption that maximum velocity and flow thickness were Rayleigh distributed.

Hughes et al. (2012) analyzed data from 9 small-scale experiments conducted by Hughes and Nadal (2009) that combined wave overtopping with a low negative freeboard with a 1-on-4.25 planar seaward slope. On the levee crest, time series of instantaneous discharge were calculated as the product of the coincident flow thickness and flow velocity time series. An analysis of nearly 2100 individual wave volumes produced a relationship between maximum instantaneous discharge and wave volume, and an associated equation for overtopping duration.

Hughes (2015a, 2015b) analyzed the extensive *FlowDike I* and *FlowDike II* data sets (described in Section 3), and he proposed new empirical equations for maximum velocity, maximum flow thickness, maximum discharge per unit crest length, and the overtopping duration occurring in individual overtopping wave volumes. Hughes noted the new equations strictly apply at the seaward edge of the dike crest on dikes having planar seaward-side slopes ranging between 1-on-3 and 1-on-6.

There has been hardly any research on the profile shape of time-varying discharge in an individual overtopping wave. Van der Meer (2007) examined raw data from the German regular wave overtopping tests provided by Dr. Schüttrumpf, and he concluded that the time variation of overtopping flow velocity, $u(t)$, and flow thickness, $h(t)$, were essentially triangular in shape for the larger overtopping wave volumes. Multiplying the velocity and flow thickness time series (assuming the maximum peaks coincide) gives the time series of instantaneous discharge that can be integrated to give total volume expressed by Van der Meer (2007) as

$$V_T = \frac{u_{max}\,h_{max}\,T_o}{3} = \frac{q_{max}\,T_o}{3} \tag{3}$$

where u_{max} is maximum flow velocity, h_{max} is maximum flow thickness, T_o is overtopping duration, and $q_{max} = u_{max}\,h_{max}$.

Hughes (2011) formulated an equation for the idealized time-varying discharge in an overtopping wave by assuming the flow thickness and flow velocity were represented by the expressions

$$h(t) = h_{max}\left[1 - \frac{t}{T_o}\right]^m \text{ For } 0 \le t \le To \tag{4}$$

and

$$u(t) = u_{max}\left[1 - \frac{t}{T_o}\right]^n \text{ For } 0 \le t \le To \tag{5}$$

where $h(t)$ and $v(t)$ are instantaneous flow thickness and velocity, respectively; t is time; and the exponents m and n are positive. Multiplying Eqs. (4) and (5) yields an equation for the time variation of instantaneous discharge given by

$$q(t) = h_{max}\,u_{max}\left[1 - \frac{t}{T_o}\right]^{m+n} = q_{max}\left[1 - \frac{t}{T_o}\right]^{m+n} \text{ For } 0 \le t \le To \tag{6}$$

Integration of Eq. (6) gives the total volume in the overtopping wave, i.e.,

$$V_T = \frac{q_{max}\,T_o}{(m+n+1)} \tag{7}$$

Hughes (2011) agreed with Van der Meer (2007) that the flow thickness and flow velocity profiles were typically well represented by triangular shapes, and he set $m = n = 1$. Thus, Eq. (7) reduced to the same as Eq. (3) proposed by Van der Meer, and Eq. (6) became

$$q(t) = q_{max}\left[1 - \frac{t}{T_o}\right]^2 \text{ for } 0 \le t \le To \tag{8}$$

Eq. (7) can be used to replace T_o in Eq. (8) yielding

$$q(t) = q_{max}\left[1 - \frac{q_{max}\, t}{3\, V_T}\right]^2 \text{ for } 0 \le t \le To \tag{9}$$

3. *FlowDike* experiment data analysis

3.1. Overview of FlowDike experiments

In this paper, data obtained from two experiments called *FlowDike 1* and *FlowDike 2* are analyzed to examine time-varying discharge in overtopping waves. The two small-scale *FlowDike* laboratory studies were conducted in a wave basin at the Danish Hydraulic Institute in Hørsholm, Denmark having a length of 35 m, a width of 25 m, and a maximum water depth of 0.9 m. An 18-m-long segmented wave generator having 36 paddles was located along a 35-m-long wall to generate long- or short-crested multidirectional waves. The *FlowDike 1* experiments were funded by the European Community through the HYDRALAB III project, and the *FlowDike 2* experiments were funded by the German Ministry of Research (BMBF) and the German Coastal Research Council (KFKI). Both experimental programs investigated wave run-up and overtopping on smooth dikes with planar seaward-side slopes.

The *FlowDike 1* tests were conducted in January 2009, and these tests used a dike with a planar seaward dike face having a slope of 1-on-3 (vertical-on-horizontal). In November 2009 the *FlowDike 2* tests were conducted using a dike with a 1-on-6 planar seaward dike slope. For both *FlowDike* test series, wave run-up was measured at one section of the model dike, and wave overtopping was measured at two other dike sections having different crest elevations of 60 cm and 70 cm. Still water depth during all tests with normally-incident waves was 50 cm for *FlowDike 1* and 55 cm for *FlowDike 2*. As expected, greater wave overtopping occurred at the 60-cm dike crest.

The entire *FlowDike* testing program included long-crested irregular waves with normal or oblique wave approach, with and without a lateral current, and with or without onshore-directed wind. Complete descriptions of both *FlowDike* experiments are given by Lorke et al. (2009) and Lorke et al. (2010). Their extensive report included the full testing program; wave, current, and wind parameters; model construction and layout; instrumentation and calibration; data collection and storage; initial data analyses; and some preliminary results.

3.2. Initial data screening

The data selected for analysis consisted of four experiments from *FlowDike 1* with seaward planar dike slope of 1-on-3 and four experiments from *FlowDike 2* having seaward slope of 1-on-6. All experiments used normally-incident long-crested irregular waves without lateral current or wind. During these tests, wave overtopping occurred at two dike sections having 60-cm and 70-cm crest elevations, respectively. Only data from the 60-cm-high dike were selected because the overtopping was more severe and many more waves overtopped the model dike. However, the overtopping data from the 70-cm-high dike certainly deserve to be analyzed in the future. Table 1 lists key parameters (in model-scale units) for the eight tests selected for analysis. In Table 1, H_{m0} is the energy-based significant wave height, T_p is the period associated with the spectral peak, $T_{m-1,0}$ is the mean spectral wave period, $L_{om-1,0}$ is the deep-water wave length (linear theory) associated with the mean spectral wave period, and N_w is the total number of waves in the experiment.

Time series of instantaneous discharge at the seaward and landward edges of the dike crest were calculated as the product of the flow thickness and horizontal velocity time series measured at those locations. A comparison of the discharge time series indicated that discharge was slightly higher at the dike crest landward edge measurement location.

Table 1
FlowDike incident wave parameters for selected experiments.

Test ID	H_{m0} (m)	T_p (s)	$T_{m-1,0}$ (s)	$L_{om-1,0}$ (m)	$H_{m0}/L_{om-1,0}$ (–)	Iribarren # (–)	N_w (–)
1-on-3 seaward dike slope (*FlowDike 1*)							
0198	0.103	1.781	1.619	4.092	0.0252	2.101	1180
0199	0.094	1.280	1.164	2.113	0.0445	1.581	1102
0200	0.150	2.156	1.960	5.996	0.0250	2.107	1276
0201	0.148	1.517	1.379	2.969	0.0499	1.493	1150
1-on-6 seaward dike slope (*FlowDike 2*)							
0451	0.090	1.710	1.555	3.772	0.0239	1.079	1097
0453	0.122	1.830	1.663	4.310	0.0282	0.992	1120
0456	0.157	2.130	1.936	5.852	0.0268	1.018	1093
0457	0.141	1.510	1.373	2.941	0.0479	0.761	1116

In addition, a velocity meter malfunction resulted in bad discharge estimates at the landward side of the dike crest during the *FlowDike 1* tests. Ultimately, the data from the seaward edge of the crest were selected because the average overtopping rates at the seaward-edge location more closely matched the discharge rates determined from the overtopping collection containers. Hughes (2015a) provided additional details of the data screening processes.

3.3. Determination of individual overtopping waves

A two-step "supervised" procedure was used to identify individual overtopping wave volumes. The first step was an automated procedure in MatLab® that performed up-crossing analysis on the seaward-side calculated discharge time series using a well-tested up-crossing subroutine. Time series zero-upcrossing points were identified, and individual waves were defined by successive upcrossings. Also, maximums between up-crossing points were identified. This method had varying degrees of success, but it served as a good initial screening of the individual wave volumes.

The time-series data point indices associated with the starting and ending point of each identified individual overtopping wave volume were then determined by scanning forward and backward in the discharge time series from each individual volume peak discharge until reaching an arbitrarily small instantaneous discharge value of $q = 0.0001$ m^3/s per m (0.1 l/s per m). The wave volume was determined as the sum of the area in the discharge time series between each wave starting and ending points. Corresponding values and locations of maximum discharge, maximum flow thickness, and maximum velocity were also determined from the associated measured time series between the same starting and ending points. The overtopping duration was determined as T_o = (ending index–starting index) $*$ dt where $dt = 1/(25\text{ Hz}) = 0.04$ s for the 1-on-3 slope data, and $dt = 1/(40\text{ Hz}) = 0.025$ s for the 1-on-6 slope data. The information for each identified wave (consecutive ID number, start index, stop index, duration, volume, maximum discharge, maximum flow thickness, maximum velocity, and other information) was written in sequential order to an ASCII-format output file for the test being analyzed.

An annotated plot of the discharge time series was produced in MatLab® as illustrated by the short section of the discharge time series shown in Fig. 1. Each identified individual wave discharge peak was automatically labelled with a sequential ID number, and the automatically-placed black circles and red squares identified the starting and ending time series indices, respectively. Sometimes the squares indicating the end of one wave volume were at nearly the same location as the black circle indicating the start of the following wave.

As seen in Fig. 1, the automated procedure succeeded for some wave volumes and failed for others. Note in particular in Fig. 1 the series of larger wave volumes. In this case, two individual waves (#69 and #70) did not have the proper start/end points determined because the discharge did not get small enough between waves to meet the selected

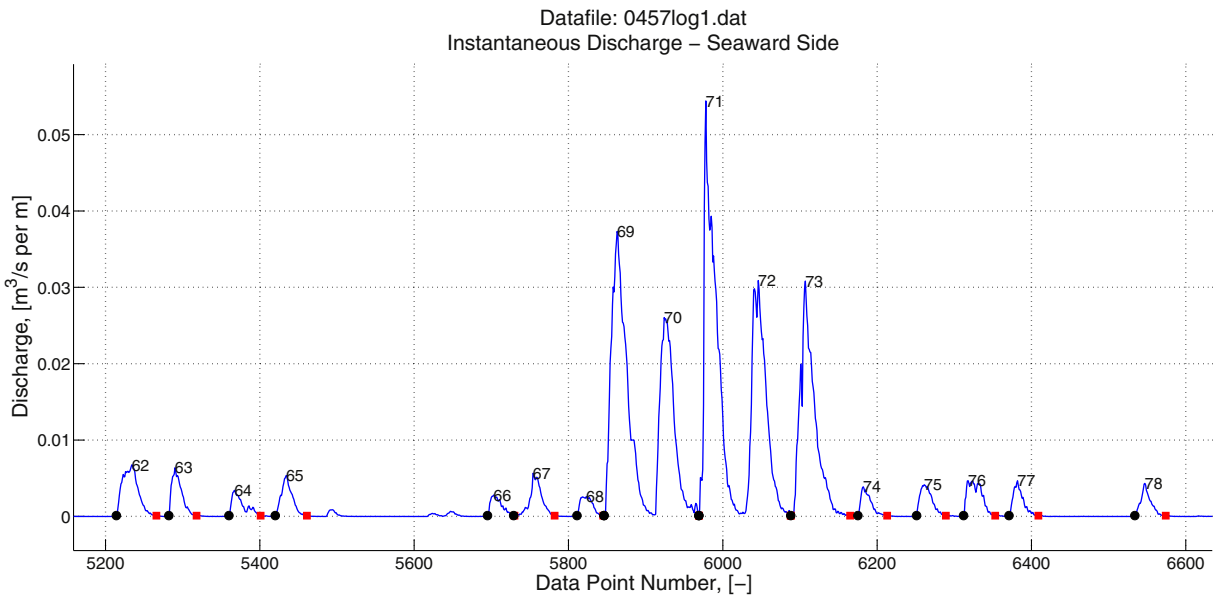

Fig. 1. Identification of individual overtopping wave volumes.

threshold criterion. Consequently, waves #69 and #70 both had identical, but incorrect, parameters listed in the output file. The volume was taken as the sum of the volumes in both waves, the duration was taken as the sum of durations for both waves, and the maximum parameters were taken as the maximum of wave #69. The same issue occurred for waves numbered #71, #72, and #73 shown in Fig. 1. Finally, some very small waves were missed altogether.

The inaccuracies encountered during the automated wave volume determination were resolved in the second step of the procedure. The annotated time-series plot of discharge was displayed on the computer screen so it could be manually scrolled through the entire annotated time series. This allowed a visual examination of every wave. Data in the automatically-produced ASCII text file corresponding to properly determined wave volumes were kept, and lines relating to incorrectly determined volumes were deleted. This first step in the supervised procedure resulted in an amended file of accurate wave volumes (and associated parameters) that had been determined automatically for each test and visually confirmed, but the file did not include all of the wave volumes from the test.

The second step in the supervised procedure was to determine manually the correct starting and ending indices for the waves that had been eliminated or missed during the first step. Additional MatLab® code was written that allowed the operator to scroll through the annotated plot of the discharge time series and manually select (with the computer mouse) the starting and ending points for any waves that were not correctly specified in the first step. After each wave selection, all the other parameters for the manually selected wave were automatically determined and saved in a second ASCII file for that experiment. The second file for each test contained all the corrected wave volumes that were either missed or incorrectly identified during the automated step. The second file of manually-determined waves was appended to the end of the first file to form a final ASCII file containing all of the wave volumes. Appending the manually-determined wave volumes file behind the corrected automatically-determined wave volumes file resulted in a combined file of all wave volumes that are not in exact sequential order. Strict chronological ordering was not necessary for the analyses presented in this paper. However, if strict time sequencing of the wave volumes is needed for any reason, it is an easy task to sort the rows (wave volumes) in the data files according to the starting index. Generally, the manual process was most useful for correcting the larger wave volumes and including the smallest wave volumes that were often missed by the automated procedure. These are important waves to be included in the data set.

A final check of the supervised wave volume determination methodology was performed by estimating the average discharge for each test as the sum of the individual wave volumes divided by the total test time. These volume-based average discharges are compared in Table 2 to the average discharges calculated directly from the discharge time series for all selected tests at the seaward edge of the 60-cm dike. The second column is the discharge determined from the time series, the third column is discharge determined from the individual wave volumes, and the fourth column is the average of columns 2 and 3. The average discharges determined from the discharge time series were just slightly greater in all cases, and this was probably due to the omission of several very small wave volumes during the manual phase of wave volume determination. Nevertheless, the minor difference between the two estimates lends confidence to the veracity of the individual wave volume data.

The rightmost three columns of Table 2 summarize the number of waves correctly identified by the automatic procedure, the number of waves that were manually-determined for each *FlowDike* test, and the total number of waves for each test. A total of 2670 individual wave

Table 2
Average discharges and summary of supervised wave volume determination.

Test ID	Average overtopping discharge			Number of individual wave volumes		
	q_w from time series (l/s per m)	q_w from wave volumes (l/s per m)	Average q_w (l/s per m)	Automatic determined volumes	Manually determined volumes	Total individual volumes
1-on-3 seaward dike slope (*FlowDike 1*)						
0198	1.942	1.934	1.938	486	177	663
0199	0.850	0.842	0.846	211	235	446
0200	4.794	4.775	4.784	453	361	814
0201	3.393	3.389	3.391	254	493	747
Total wave volumes						2670
1-on-6 seaward dike slope (*FlowDike 2*)						
0451	0.608	0.605	0.606	535	46	581
0453	1.632	1.648	1.640	726	142	868
0456	4.283	4.269	4.276	617	275	892
0457	1.851	1.838	1.844	521	267	788
Total wave volumes						3129

volumes were determined for *FlowDike 1* that used the 1-on-3 seaward slope, and 3129 wave volumes were determined for the 1-on-6 seaward slope from the *FlowDike 2* tests. This gave a grand total of 5799 individual wave volumes suitable for additional analyses.

4. Proposed time-varying theoretical equations

The time variation of instantaneous discharge in individual overtopping waves typically features a rapid increase in discharge to a maximum value, followed by a slower decline in discharge down to zero. Examination of many individual overtopping waves indicated that the time-varying discharge at a fixed location resembles somewhat the mathematical form of the familiar two-parameter Weibull probability density function. Likewise, the time-varying cumulative overtopping wave volume, obtained as the stepwise integration of the instantaneous discharge, resembles the associated Weibull cumulative probability distribution function, which is of course, the integration of the probability density function.

4.1. Time-varying discharge and cumulative overtopping volume

Adopting the mathematical forms of the Weibull probability density function and cumulative probability distribution function, respectively, to represent the time-varying discharge and cumulative overtopping wave volume results in the following equations

$$q(t) = \frac{V_T\, b}{a}\left(\frac{t}{a}\right)^{(b-1)} exp\left[-\left(\frac{t}{a}\right)^{b}\right] \tag{10}$$

and

$$V(t) = V_T\left\{1-\exp\left[-\left(\frac{t}{a}\right)^{b}\right]\right\} \tag{11}$$

In Eqs. (10) and (11), $q(t)$ is instantaneous discharge per unit dike length, $V(t)$ is cumulative overtopping volume per unit dike length, V_T is total wave volume per unit length, t is time, a is the distribution scale factor, and b is the distribution shape factor. The total wave volume per unit length, V_T, is included so the cumulative wave volume is equal to total wave volume when t approaches infinity, i.e., $V(t\to\infty) = V_T$. Eqs. (10) and (11) revert to the familiar Rayleigh form of the equations when the shape factor, $b = 2$. It is easy to verify that Eq. (10) is the derivative of Eq. (11).

4.2. Features of the proposed time-varying equations

A few characteristic features of the overtopping wave time-varying discharge distribution and time-varying cumulative overtopping volume being represented by the Weibull equations can be easily derived. The time at the occurrence of the maximum (or peak) discharge is found by differentiating Eq. (1) and setting the result equal to zero. After some algebraic manipulation, the theoretical time at maximum discharge, t_{maxT}, is given by

$$t_{maxT} = a\left(\frac{b-1}{b}\right)^{1/b} \tag{12}$$

where the upper-case "*T*" is used in the subscript (here and in subsequent equations) to denote "*theoretical*." Substituting t_{maxT} from Eq. (12) for t in Eq. (10) yields an expression for the theoretical maximum discharge in an overtopping wave, i.e.,

$$q_{maxT} = \frac{V_T\, b}{a}\left(\frac{b-1}{b}\right)^{\frac{b-1}{b}} exp\left[-\left(\frac{b-1}{b}\right)\right] \tag{13}$$

An approximation of the total overtopping duration can be estimated from the cumulative overtopping volume Eq. (11) by calculating the time it takes for the cumulative volume to reach (say) 99% of the total volume. In other words,

$$V(t = T_{oT}) \approx 0.99\, V_T = V_T\left\{1-exp\left[-\left(\frac{T_{oT}}{a}\right)^{b}\right]\right\} \tag{14}$$

Of course, it would be reasonable to select some other arbitrary total volume percentage (say 95% or 99.9%) to define the overtopping duration. Solving Eq. (14) for T_{oT}, and noting that mean discharge in an individual overtopping wave can be defined as total overtopping wave volume divided by overtopping duration, yields an approximate equation for theoretical mean overtopping discharge in an individual overtopping wave given by

$$q_{meanT} = \frac{V_T}{T_{oT}} = \frac{V_T}{a\ [-\ln(0.01)]^{1/b}} \tag{15}$$

The value of mean discharge given by Eq. (15) is strictly for a single overtopping wave, and it should not be confused with the average

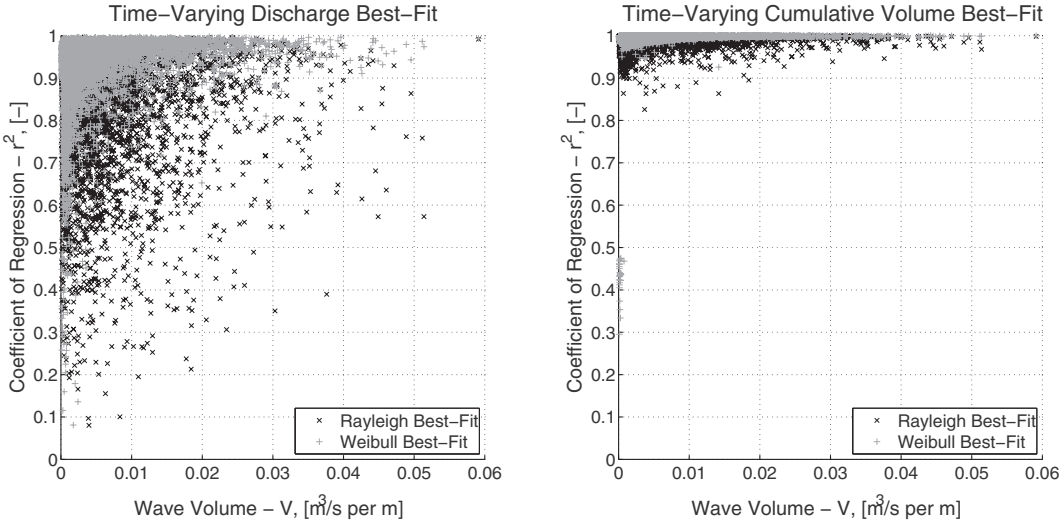

Fig. 2. Comparison of r^2 values for best-fits using Rayleigh and Weibull equations.

overtopping discharge, q_w, of the storm event. Eqs. (12)–(15) reduce to the Rayleigh equation versions when the shape factor, $b = 2$.

5. Best-fits to measured data

Each individual overtopping wave in the discharge time series was characterized by the evenly-spaced discharge points located between the wave starting and ending indices. The corresponding time series of cumulative overtopping volume was calculated as the cumulative summation of instantaneous discharge at each point between starting and ending indices multiplied by the incremental time between measurement points. Non-linear least-squares best-fits of the proposed Weibull instantaneous discharge distribution (Eq. 10) and the corresponding Rayleigh version ($b = 2$) of Eq. (10) were performed using as the target the time-varying instantaneous discharge measurements for all 5799 individual overtopping waves. Similarly, best-fits of the proposed Weibull cumulative volume distribution (Eq. 11) and the Rayleigh version of Eq. (11) were performed using the time-varying cumulative overtopping volume as the target. Thus, the best-fit analysis gave a total of $4 \times 5799 = 23{,}196$ least-squares best-fit results for the *FlowDike* data set.

5.1. Quality of best-fits

The quality of the best-fits was indicated by the square of the correlation coefficient (sometimes referred to as the coefficient of determination) defined as

$$r^2 = \frac{SSR}{SSE + SSR} \tag{16}$$

where *SSR* is the "sum of squared residuals" and *SSE* is the "sum of squared errors." The coefficient of determination is interpreted as the proportion of the variance in the dependent variable that is predictable from the independent variable. For best-fits of the time-varying discharge equation OR the time-varying cumulative volume equation the quantities *SSR* and *SSE* are given by the following equations

$$SSR = \sum_{i=1}^{N} (q_i - \overline{q}_m)^2 \quad \text{or} \quad SSR = \sum_{i=1}^{N} (V_i - \overline{V}_m)^2 \tag{17}$$

and

$$SSE = \sum_{i=1}^{N} (q_i - q_{m.i})^2 \quad \text{or} \quad SSE = \sum_{i=1}^{N} (V_i - V_{m.i})^2 \tag{18}$$

where

q_i = best-fit value of instantaneous discharge at time increment i
$q_{m,i}$ = measured instantaneous discharge at time increment i
$\overline{q}_m$ = mean of measured instantaneous discharges in wave
V_i = best-fit value of cumulative wave volume at time increment i
$V_{m,i}$ = measured cumulative wave volume at time increment i
$\overline{V}_m$ = mean of measured cumulative volume in wave
N = total number of increments in overtopping wave.

Values of the coefficient of determination, r^2, as a function of individual wave volume for all 5799 wave volumes are shown in Fig. 2 for both the Rayleigh (black markers) and Weibull (gray markers) versions of the equations. The left-hand plot of Fig. 2 compares r^2 values for the time-varying discharge (Eq. 10). The mean value of the coefficient of determination was $r^2 = 0.860$ for the Rayleigh discharge equation, and $r^2 = 0.932$ for the Weibull discharge equation, both of which are judged

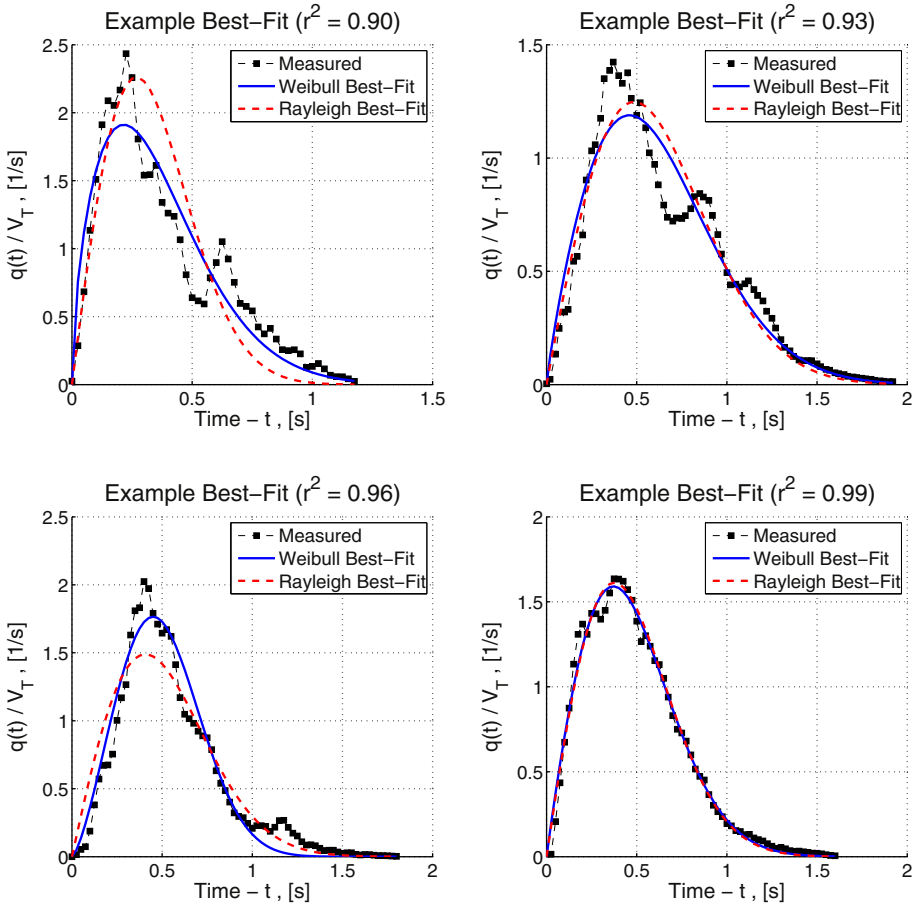

Fig. 3. Best-fit examples for Rayleigh and Weibull time-varying discharge equations.

to be very good. The right-hand plot of Fig. 2 compares r^2 values for the time-varying cumulative overtopping volume (Eq. 11). The mean value of the coefficient of determination was $r^2 = 0.988$ for the Rayleigh cumulative volume equation, and $r^2 = 0.992$ for the Weibull cumulative volume equation indicating an excellent fit to the data. In many, but not all, cases the Weibull versions of the equations provided a better fit to the measured data. Obviously, the equations for cumulative overtopping volume gave the best fits.

Fig. 3 shows four best-fit examples of the Rayleigh and Weibull versions of the time-varying discharge equation (Eq. 10) compared to the associated individual wave measured discharge. The individual waves were selected to illustrate best-fits having progressively better r^2-values (based on the Weibull version of Eq. (10)). Note that maximum (or peak) discharge of the theoretical time-varying discharge is typically less than the measured maximum peak. The comparison shown on the upper right-hand plot of Fig. 3 has an r^2-value equal to the mean of all 5799 best-fits of the Weibull version of Eq. (10). Best-fits of the Rayleigh version of the discharge distribution equation differed somewhat for the two cases shown on the upper-left and lower-left plots, but the difference was quite small for the plots shown on the upper- and lower-right side of Fig. 3. The almost exact match between Raleigh and Weibull shown on the lower-right plot of Fig. 3 is a case where the best-fit value of the shape factor was nearly $b = 2$. Whereas the best-fits of the Weibull version of the discharge equation was expected to be better, in many cases the simplified Rayleigh version provided reasonable results.

5.2. Best-fit scale factors, a

The left-hand plot of Fig. 4 compares values of the scale factor, a_{Rq}, obtained from the best-fits of the Rayleigh version of the time-varying discharge (Eq. 10) to the corresponding scale factors, a_{Wq}, obtained from best-fits of Weibull version of Eq. (10). The two seaward-side slopes are denoted by different marker types, and the solid line is the line of equivalence. There is slightly more scatter for the steeper 1-on-3 slope. A similar comparison is shown on the right-hand plot of Fig. 4 for best-fit scale factors determined from the Rayleigh version (a_{RV}) and the Weibull version (a_{WV}) of the time-varying cumulative overtopping volume equation (Eq. 11). Both comparisons are very good with nearly perfect correspondence shown for the cumulative overtopping equation. These comparisons indicate that the value of shape factor, b, has little influence on scale factor, a, because the shape factor was allowed to vary for the Weibull version best-fits, but was held constant for the Rayleigh version best-fits.

Fig. 5 compares scale factors determined from the time-varying discharge equation to those determined from the time-varying cumulative overtopping equation for both the Rayleigh and Weibull versions. The plot shows fairly good correspondence between the discharge equation and the cumulative volume equation best-fit values for scale factor. This implies that similar values of scale factor, a, can be obtained from using either the Rayleigh or Weibull versions of Eq. (10) or Eq. (11). This finding greatly facilitates establishing an empirical correlation for the scale factor. In just a relatively few instances, scale factors determined by the two equations do not correspond as indicated by the outlying data points on Fig. 5. The cause for this disagreement lies in the fact that a small minority of the calculated individual wave time-varying discharge time series had bizarre shapes or the start/stop points were not correctly determined by the automatic/supervised procedure. In the case of time series shapes significantly different from the theoretical assumption, the scale factor determined from cumulative overtopping would tend to be the more correct of the two.

5.3. Best-fit shape factors, b

The Weibull shape factor, b_q, obtained from the best-fit of Eq. (10) is compared to the corresponding shape factor (b_V) from the best-fit of Eq. (11) in Fig. 6. Data from the two different seaward-side slopes are shown by different markers, and the solid line is the line of equivalence. Scatter in the comparison is greater for the steeper 1-on-3 slope data. In the overwhelming majority of cases, larger shape factors resulted from the best-fits of the time-varying discharge equation (Eq. 10) to the data as opposed to best-fits from the time-varying cumulative volume equation (Eq. 11). Thus, a definite bias exists in the magnitude of the shape factor depending on which equation is used for the best-fit. This bias hinders discovering an empirical representation for shape factor because (theoretically) the shape factor should be the same for both the time-varying discharge equation and the time-varying cumulative overtopping volume equation.

In summary, it has been shown that the proposed two-parameter Weibull equations for the time variation of instantaneous discharge and cumulative overtopping volume provide reasonably good approximation of measured time-dependent overtopping volumes measured during the *FlowDike* experiments. Furthermore, the one-parameter Rayleigh versions of the same equations with $b = 2$ provided best-fits that were nearly as good as the two-parameter Weibull equations in many cases.

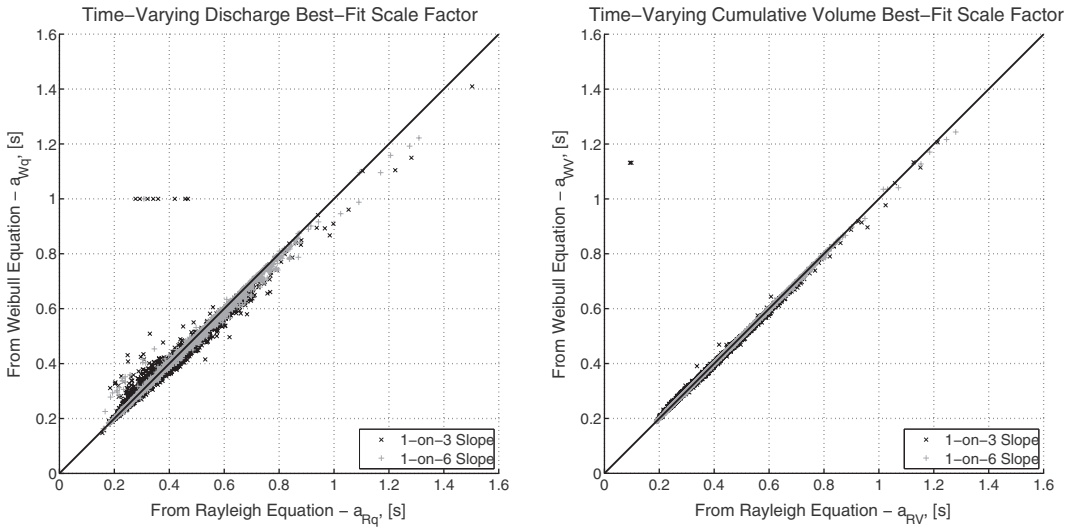

Fig. 4. Comparisons of best-fit scale factor, a, obtained time-varying discharge and cumulative volume equations.

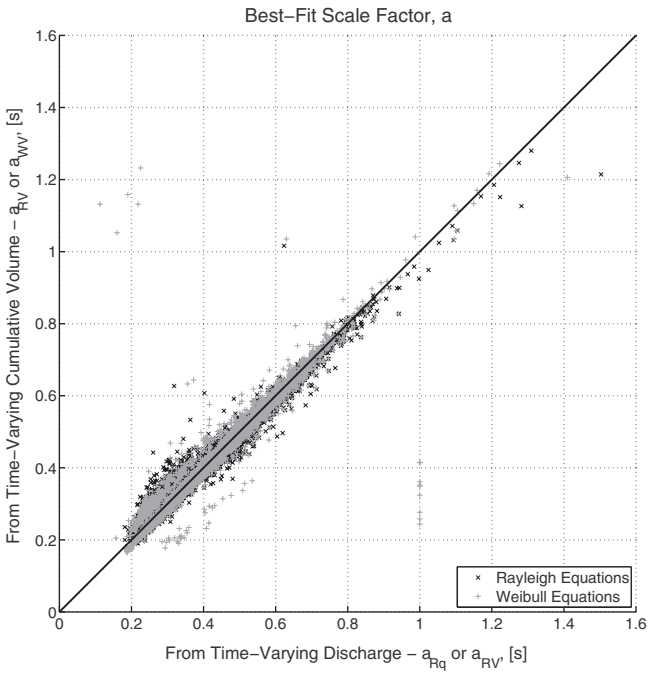

Fig. 5. Comparison of all best-fit scale factors, *a*.

6. Correlations for Weibull parameters

The theoretical equations for time-varying discharge and cumulative volume in overtopping waves (Eqs. 10–15) require appropriate values of the scale factor, *a*, and the shape factor, *b*, expressed in terms of predictable key parameters of individual overtopping waves. Ideally, the approach would be to consider two of the equations derived from the theoretical time-varying Weibull equations: the theoretical maximum discharge, q_{maxT}, (Eq. 13), and the theoretical mean discharge, q_{meanT}, (Eq. 15). Assuming that q_{maxT} and q_{meanT} can be appropriated in terms of overtopping wave parameters, Eqs. (13) and (15) are two equations

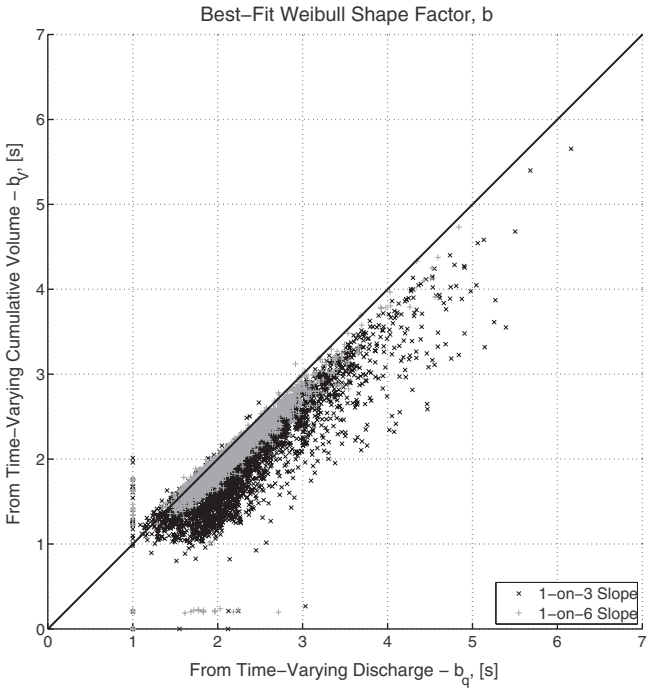

Fig. 6. Comparison of best-fit shape factors, *b*.

with two unknowns, *a* and *b*. However, both equations are transcendental forms in terms of the unknowns, so a simple algebraic solution was not possible.

6.1. Correlation for scale factor, a

The scale factor, *a*, in the Weibull distribution is an indicator of the spread of the distribution independent variable. In the case of Eqs. (10) and (11), the independent variable is time; and the scale factor is most closely related to the duration of overtopping, T_o. Larger values of scale factor give larger values of T_o. The best-fit scale factors, *a*, were shown in Figs. 4 and 5 to be quite similar irrespective of which equation was used for the best-fit (time-varying discharge or cumulative volume) and whether or not the Raleigh or Weibull version was applied. This observation simplifies the correlation for the best-fit shape factor because it appears that shape factor, *b*, does not influence the value of scale factor, *a*. Thus, it seems reasonable to use the Rayleigh version of Eq. (15) with $b = 2$ for mean overtopping discharge because: (a) the cumulative volume equation is based on the overtopping duration, T_{oT}, which is closely related to scale factor; and (b) the shape factor has little influence on scale factor. *Re*-arranging Eq. (15) and using the Rayleigh version assumption of $b = 2$ yields an equation for scale factor in terms of individual overtopping wave volume (V_T) and theoretical mean overtopping discharge (q_{meanT}), i.e.,

$$a_T = \frac{V_T}{q_{meanT}\ [-\ln(0.01)]^{1/2}} \qquad \text{which is equivalent to} \qquad (19)$$

$$a_T = \frac{V_T}{q_{meanT}\ (2.146)}$$

where a_T represents the theoretical shape factor.

Mean discharge per unit dike length was calculated for all 5799 individual overtopping waves as the average of all the time-varying discrete discharge values measured in the wave, and a correlation was sought in terms of overtopping wave parameters. It appeared that mean discharge was chiefly a function of wave volume only, and dimensional analysis suggested that wave volume should be raised to the 3/4-power for dimensional consistency. The plot in Fig. 7 shows calculated mean discharge of the measured data plotted versus the parameter $\sqrt{g}\ V_T^{3/4}$. (Gravity was included in the parameter to balance the dimensions.) The straight line on the Fig. 7 plot is a linear regression forced through the origin given by the equation

$$q_{mean} = 0.066\ \sqrt{g}\ V_T^{3/4} \qquad (20)$$

where *g* is gravitational acceleration and V_T is the total volume in an individual overtopping wave. This best-fit equation had a correlation coefficient of $C_c = 0.978$, a coefficient of determination of $r^2 = 0.956$, and a root-mean-square error of $E_{RMS} = 0.0008$ m^3/s per m, indicating an excellent representation of the equation to the data. Eq. (20) should be considered tentative, and application of this equation would not be appropriate for seaward-side slopes that are not planar or for planar slopes outside the range of $1/3 > \tan\alpha > 1/6$.

Substituting the measured mean discharge given by Eq. (20) for the theoretical mean discharge in Eq. (19) yields the empirical equation

$$a_E = \frac{7.06\ V_T^{1/4}}{\sqrt{g}} \qquad (21)$$

where a_E is an empirical approximation of the theoretical scale factor. The empirical scale factor given by Eq. (21) is plotted versus the best-fit scale factor, a_{RV}, obtained from the Rayleigh version of the time-varying cumulative volume equation on the left-hand plot of Fig. 8. The diagonal line is the line of equivalence, and there is certainly more scatter in the data from the 1-on-3 seaward-side slope.

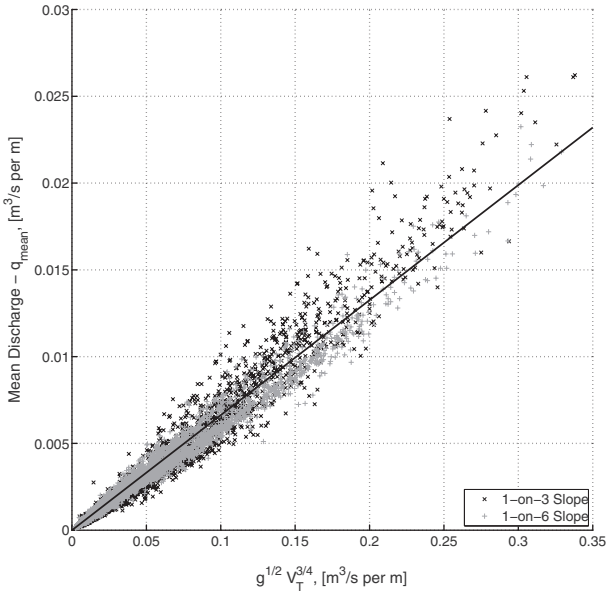

Fig. 7. Correlation of mean discharge, q_{mean}, to wave overtopping volume, V_T.

Further investigation suggested that a better result could be obtained if the seaward-side dike slope was included in the empirical formulation. The analysis resulted in the following best-fit empirical equation for scale factor

$$a_E = \frac{2.44\, V_T^{1/4}}{\sqrt{g\, tan\alpha}} \tag{22}$$

where α is the angle of the seaward-side dike slope relative to the horizontal. This best-fit equation had less favorable fit parameters of a correlation coefficient of $C_c = 0.692$, a coefficient of determination of $r^2 = 0.480$, and a root-mean-square error of $E_{RMS} = 0.107$ s. Estimates of a_E from Eq. (22) are plotted versus the corresponding best-fit scale factors, a_{RV}, on the right-hand plot of Fig. 8. Naturally, the correlation between empirical and best-fit scale factors exhibits scatter, but the general trend is seen to be representative of the 5799 measured individual overtopping waves. The scatter shown on Fig. 8 represents the combined uncertainty present in both the data itself and in the empirical representation of the measured mean discharge (q_{mean}) as exhibited in Fig. 7.

6.2. Correlation for shape factor, b

The shape factor, b, in the Weibull distribution affects the shape of the distribution, and it is equivalent to the slope of the cumulative distribution when plotted on probability paper. For the time-varying discharge (Eq. 10) the shape factor influences the peak discharge and the narrowness of the time-varying discharge peak. Fig. 9 compares the theoretical time-varying discharge for a wave overtopping a 1-on-3 seaward slope with an overtopping volume of $V_T = 5.5$ m^3/m (the maximum of the Dutch wave overtopping simulator). The appropriate scale factor of $a = 2.07$ s was determined using Eq. (22). Three values of shape factor are plotted, including $b = 2.0$ (Rayleigh version). Increasing the shape factor increases the magnitude and time of the maximum discharge, resulting in more peakedness in the distribution of time-varying discharge.

An attempt was made to develop an empirical representation of the shape factor using the theoretical equation for maximum discharge, q_{max} (Eq. 13). Unfortunately, the resulting correlation exhibited excessive scatter caused by the combination of uncertainty in the best-fit values of b, uncertainty in the correlation for q_{max} in terms of wave volume, and uncertainty in the scale factor (as seen in Fig. 8). In fact, the correlation for shape factor was so poor that predictions of measured time-varying discharge using the Rayleigh version of the equation were better than predictions using the Weibull version with the faulty estimate of shape factor.

The distribution of the best-fit shape factors are shown on Fig. 10 with the left-hand plot obtained from best-fits of the time-varying discharge equation and the right-hand plot obtained from best-fits of the cumulative overtopping volume equation. In both instances, the shape factors are narrowly distributed about mean values near $b = 2$, which is the Rayleigh simplification. The standard deviations shown on Fig. 10 are included only to give a sense of the narrowness of the distributions about the mean values, and not for any analytical application.

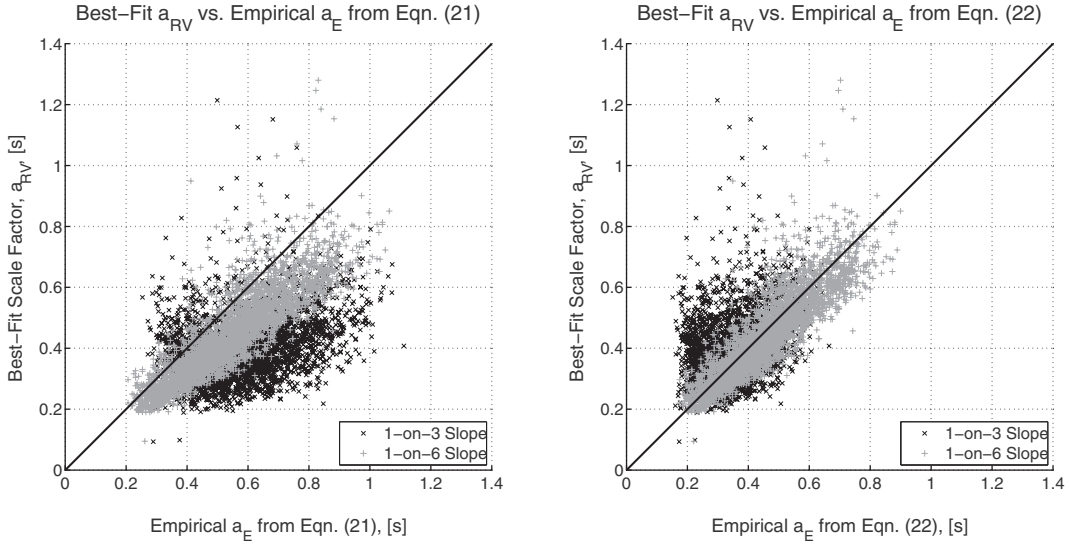

Fig. 8. Correlation for Weibull scale factor, a.

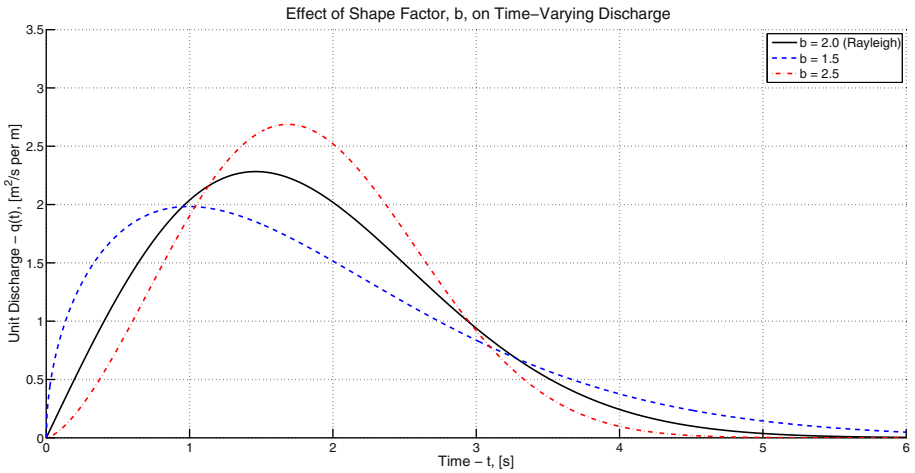

Fig. 9. Effect of Weibull shape factor, *b*, on theoretical time-varying discharge.

Future efforts may result in a more meaningful representation for the shape factor, but in the meantime we believe the Rayleigh value of $b = 2$ should be used in the theoretical equations (Eqs. 10–15).

7. Time-varying discharge prediction assessment

Predictions of the time-varying discharge and time-varying cumulative overtopping volume were made using Eqs. (10) and (11), respectively. Scale factor, *a*, was determined using Eq. (22), and the shape factor was fixed at $b = 2$. The root-mean-square (RMS) errors associated with the best-fits to measured data and predictions to measured data were calculated for the time-varying discharge and the time-varying cumulative overtopping volume as

$$E_{RMS} = \sqrt{\frac{\sum_{i=1}^{N}\left(q_i - q_{m,i}\right)^2}{N}} \quad or \quad E_{RMS} = \sqrt{\frac{\sum_{i=1}^{N}\left(V_i - V_{m,i}\right)^2}{N}} \tag{23}$$

where

q_i = best-fit (or predicted) value of instantaneous discharge at time increment *i*
$q_{m,i}$ = measured instantaneous discharge at time increment *i*
V_i = best-fit (or predicted) value of cumulative wave volume at time increment *i*
$V_{m,i}$ = measured cumulative wave volume at time increment *i*
N = total number of increments in overtopping wave.

Average RMS errors for best-fits and predictions are listed on Table 3. For the best-fits, the Weibull versions of the equations provided smaller RMS errors than the corresponding Rayleigh versions. RMS errors for the predictions were larger, but not by a large margin.

Example predictions of time-varying discharge using Eq. (10) with $b = 2$ and scale factor determined by Eq. (22) are given in Fig. 11 for the same four waves shown in Fig. 3. The predictions seem to provide a reasonable approximation of the measurements, except perhaps in the lower left-hand plot of Fig. 11. As noted previously, the predicted magnitudes of the peak (maximum) discharge are usually less than the measured peaks.

Expressions for the predicted theoretical maximum discharge and time of maximum discharge are given by Eqs. (13) and (12), respectively, with $b = 2$ and scale factor, *a*, provided by Eq. (22). Making these substitutions into Eqs. (13) and (12) yields the predictive equations

$$q_{maxT} = 0.352\, V_T^{3/4} \sqrt{g \tan\alpha} \tag{24}$$

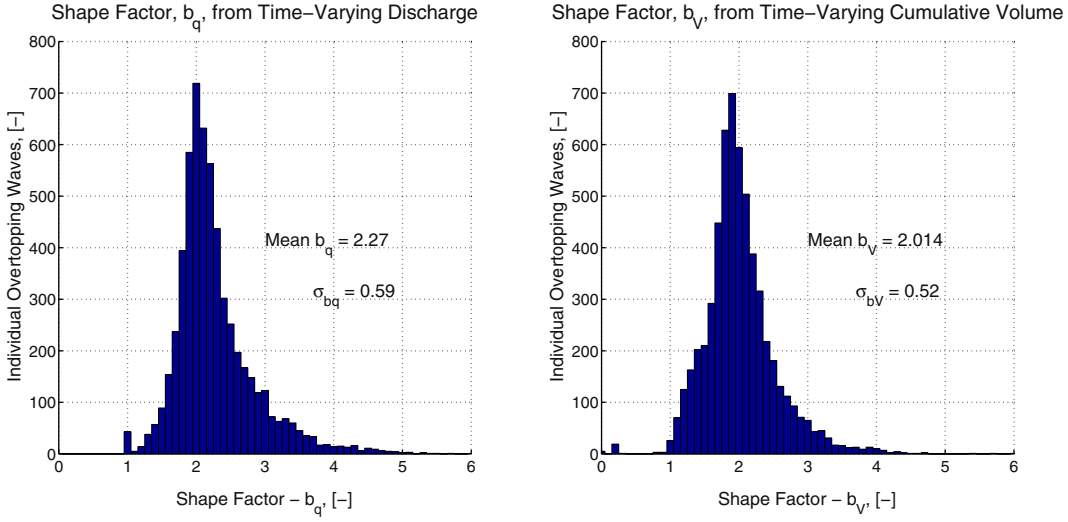

Fig. 10. Distribution of best-fit Weibull shape factor, *b*.

Table 3
Average root-mean-square errors of best-fits and predictions.

Method	Mean E_{rms}/q_{max}		Mean E_{rms}/V_T	
	Rayleigh Eq. (10)	Weibull Eq. (10)	Rayleigh Eq. (11)	Weibull Eq. (11)
Best-Fit	0.104	0.075	0.032	0.018
Prediction	0.157	–	0.079	–

and

$$t_{maxT} = \frac{1.73\, V_T^{1/4}}{\sqrt{g\, tan\alpha}} \tag{25}$$

Eqs. (24) and (25) were used to make predictions for the theoretical maximum discharge and time of occurrence; results are shown on Fig. 12. The comparison between measured maximum discharge (q_{max}) and predicted maximum discharge (q_{maxT}) is shown in the left-hand plot of Fig. 12. The line of equivalence is the dashed line, and the solid line is the best-fit line given by the empirical relationship

$$q_{max} = 1.38\, q_{maxT} \tag{26}$$

This best-fit equation had a correlation coefficient of $C_c = 0.975$, a coefficient of determination of $r^2 = 0.951$, and a root-mean-square error of $E_{RMS} = 0.0035$ m^3/s per m, which are judged to be very good. The scatter about the best-fit line is not too severe. The measured q_{max} is usually greater than the theoretical estimate based on the Rayleigh version of the equations because the shape factor was fixed at $b = 2$, and this limited the overall ability of the theoretical equation to predict the peak values while still representing the overall shape of the time-varying discharge. The comparison between measured and theoretical peak discharge would have been better if the shape factor for the two-parameter Weibull equation had been successfully parameterized.

The comparison between measured time of maximum discharge (t_{max}) and prediction (t_{maxT}) using Eq. (25) was not as good as seen on the right-hand plot of Fig. 12. The solid line is a linear best-fit through the origin given by the equation

$$t_{max} = 1.044\, t_{maxT} \tag{27}$$

This best-fit equation had a relatively poor correlation coefficient of $C_c = 0.598$, a coefficient of determination of $r^2 = 0.357$, and a root-mean-square error of $E_{RMS} = 0.11$ s. There is no compelling reason to force the equation through the origin other than we lack any rationale for doing otherwise. Given the poor correlation shown by Eq. (27), it seems inappropriate to apply this equation to real-world applications.

8. Application to cumulative excess work methodology

Dean et al. (2010) examined whether flow velocity (u), shear stress ($\propto u^2$), or work ($\propto u^3$) above a given threshold was the best parameter for relating design nomograms of grass stability derived from steady overtopping measurements to the case of unsteady wave overtopping. They concluded flow work ($\propto u^3$) above a certain threshold provided the best estimator of erosion, and the concept was named "*erosional equivalence*". Summing the individual contributions from all the overtopping waves led to the term "*cumulative excess work*" (CEW), which is quite similar to the concept of *hydraulic loading* developed by Van der Meer et al. (2010).

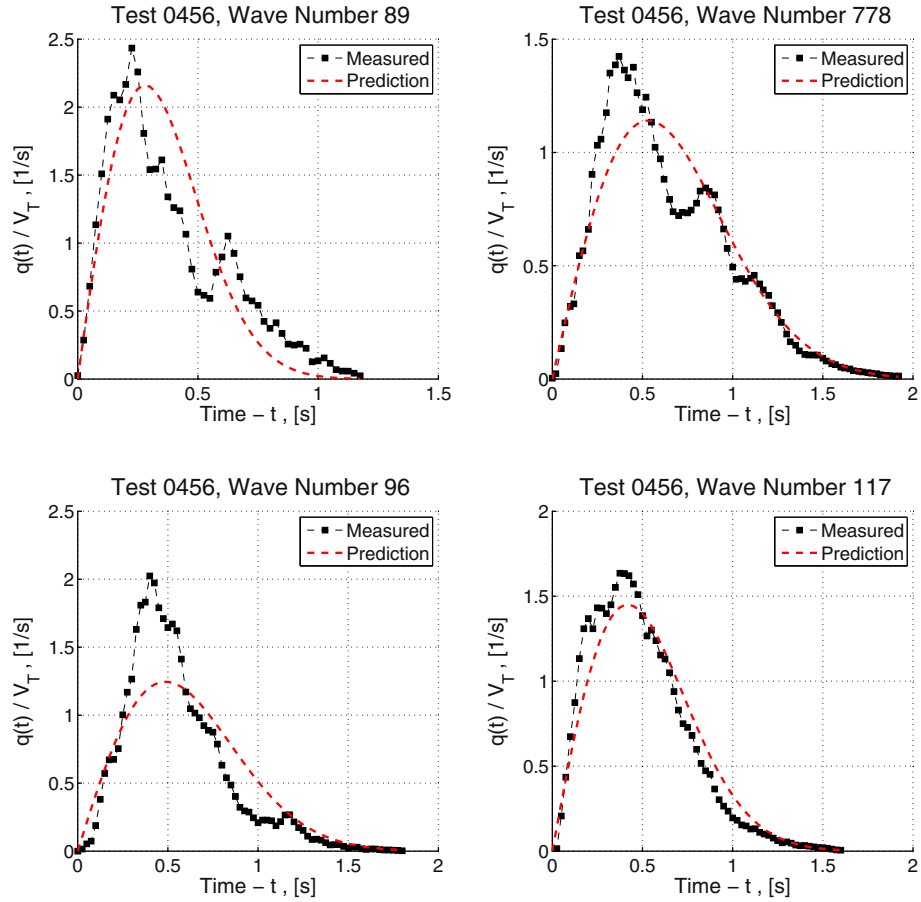

Fig. 11. Example predictions for Rayleigh time-varying discharge equation.

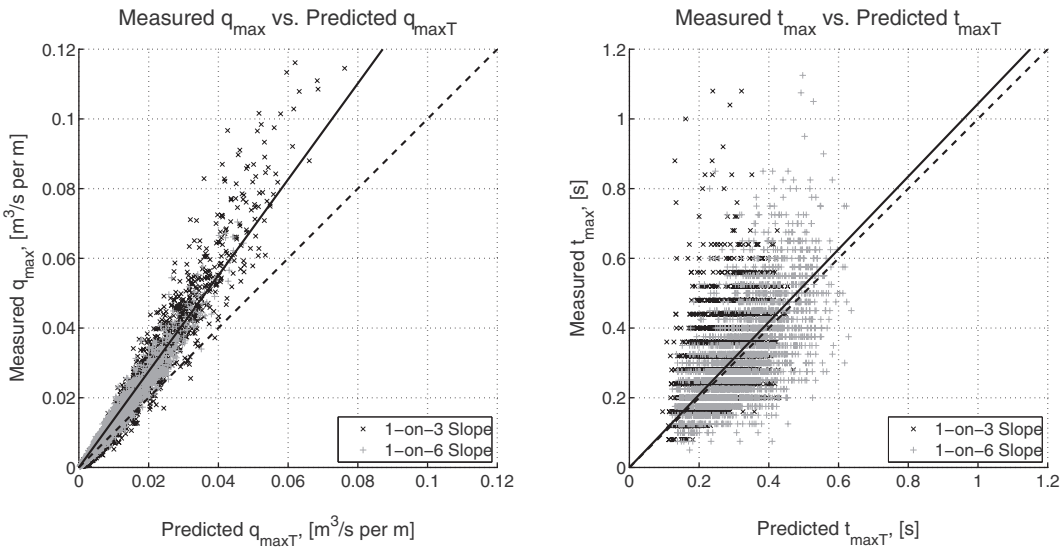

Fig. 12. Predicted magnitude and time of maximum discharge in overtopping waves.

Hughes (2011) expanded Dean et al.'s concept by showing the excess work in the overtopping wave can represented by the sum of the time-varying discharge above a critical discharge threshold, i.e.,

$$W_E = \int_{T_A}^{T_B} [q(t) - q_c]dt = V_E \text{ For } q(t) \geq qc \tag{28}$$

where W_E is excess flow work in an overtopping wave, q_c is critical threshold discharge, T_A is the time when instantaneous discharge first exceeds critical discharge, T_B is the time when instantaneous discharge again equals critical discharge, and V_E is excess volume in an overtopping wave. In other words, the excess work in an overtopping wave is equivalent to the wave volume above the critical discharge threshold shown in the time-varying discharge plot.

Hughes (2011) developed a predictive model for the cumulative excess work by assuming the idealized saw-tooth shape for the time-varying instantaneous discharge given by Eq. (9). However, the prediction equation for time-varying discharge given in this paper provides a more realistic representation that can be used in the CEW methodology. The plot in Fig. 13 illustrates cumulative excess work (or volume) using the time-varying discharge predicted by Eq. (10) for a wave volume equal to the maximum of the Dutch overtopping simulator (V_T = 5.5 m^3/m) with a 1-on-3 seaward dike slope. The scale factor, a_E, was estimated by Eq. (22), and a constant shape factor of $b = 2$ was used. The critical discharge, shown by the horizontal line, is approximately equivalent to a critical velocity of 6 m/s on a 1-on-3 landward-side dike slope where the Fanning friction factor is approximately 0.015. The wave volume per unit dike length above the critical discharge line is the excess volume (or work) that contributes to landward-side slope erosion. The excess volume is equal to 3.41 m^3/m, which is 62% of the total wave volume.

Fig. 14 presents results of similar calculations for the same dike geometry and friction factor with a range of overtopping volumes (V_T) and critical erosion velocities (u_c). The vertical axis is the ratio of excess work (volume) to total overtopping volume, i.e., V_E/V_T. The five curves represent different values of critical velocity, and marker indicates the parameters of the example given in Fig. 13. The plots in Fig. 14 indicate that a greater percentage of the work in the overtopping wave contributes to slope erosion as the critical velocity decreases and/or as the wave volume increases. Further details of the cumulative excess work concept and suggested implementation into a predictive model are given in Hughes (2011).

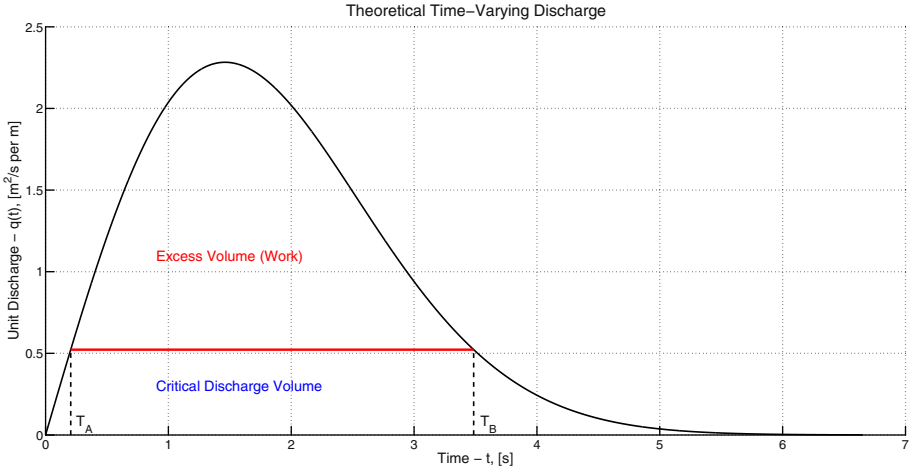

Fig. 13. Example of excess work (volume) above the threshold discharge in overtopping wave.

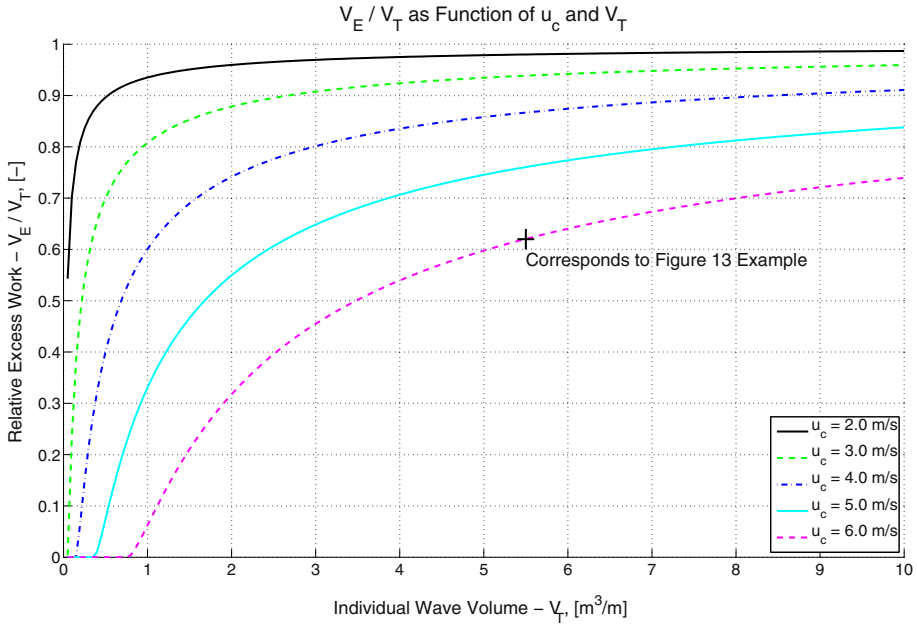

Fig. 14. Fraction of excess work (volume) in a wave volume as a function of critical erosion velocity.

9. Conclusions

This study examined time series of instantaneous discharge associated with individual overtopping waves that were measured at the seaward edge of a laboratory-scale dike crest for incident wave conditions impinging on either a 1-on-3 or 1-on-6 planar seaward-side dike slope. The shapes of the time-varying discharge and time-varying cumulative volume (per unit dike length) were well described by the two-parameter Weibull equations, as shown by nonlinear best-fits to measurements from 5799 overtopping waves. The related one-parameter Rayleigh equations with shape factor, $b = 2$, did almost as well.

A reasonable empirical equation was determined that related the best-fit values of the theoretical Weibull scale factor, a, to the individual overtopping wave volume and the seaward-side slope of the dike. However, similar success was not achieved in finding a suitable empirical relationship for the best-fit values of the Weibull shape factor, b. However, it was noted that the values of the best-fit Weibull shape factors were distributed about a peak value in the vicinity of $b = 2$, which is the shape factor for the related Rayleigh version of the Weibull equations. Consequently, it is proposed that the time-varying discharge per unit dike length (Eq. 10) and the time-varying cumulative volume per unit dike length (Eq. 11) use a shape factor of $b = 2$, along with the scale factor, a, given by Eq. (22). Assessment of the root-mean-square errors between predictions and measurements indicated the one-parameter Rayleigh versions of the equations provided reasonable estimates of the time-varying discharge, and an empirical equation provided good predictions of the maximum discharge in an individual overtopping wave.

The new equations presented in this paper strictly apply at the seaward edge of the dike crest on dikes having planar seaward-side slopes ranging between 1-on-3 to 1-on-6 (vertical-on-horizontal). These equations may prove useful for additional refinements to the science of full-scale wave overtopping simulation with the goal of providing even more realistic replication of full-scale wave overtopping by better representing the time-varying discharge at the seaward edge of the dike crest. The new formulations can also be applied in the cumulative excess work methodology for assessing the erosional resiliency of earthen dike landward-side slopes subjected to wave overtopping. Finally, it would be possible to use the developments in this paper to provide estimates of the time variation of shear stress acting on levee and dike crests for individual waves, or to evaluate risk to people or infrastructure due to overtopping waves.

List of symbols

a	=	Scale factor in Weibull equation [s]
a_E	=	Empirical scale factor [s]
a_{Rq}	=	Scale factor obtained from best-fits of time-varying Rayleigh discharge equation [s]
a_{RV}	=	Scale factor obtained from best-fits of time-varying Rayleigh cum. overtopping equation [s]
a_T	=	Theoretical scale factor [s]
a_{Wq}	=	Scale factor obtained from best-fits of time-varying Weibull discharge equation [s]
a_{WV}	=	Scale factor obtained from best-fits of time-varying Weibull cum. overtopping equation [s]
b	=	Shape factor in Weibull equation [−]
b_q	=	Shape factor obtained from best-fits of time-varying Weibull discharge equation [−]
b_V	=	Shape factor obtained from best-fits of time-varying Weibull cum. overtopping equation [−]
$C_{A,h}$	=	Empirical coefficient in $h_{2\%}$ equation [−]
$C_{A,u}$	=	Empirical coefficient in $u_{2\%}$ equation [−]
C_c	=	Correlation coefficient [−]
E_{RMS}	=	Root-mean-square error [m^3/s per m or m^3/m or s, depending of usage]
g	=	Acceleration of gravity [m/s^2]
H_{m0}	=	Energy-based significant wave height [m]
$h(t)$	=	Time-varying overtopping flow thickness perpendicular to dike surface [m/s]
h_{max}	=	Maximum instantaneous flow thickness in an overtopping wave [m]
$h_{2\%}$	=	Flow depth at seaward side of dike crest exceeded by 2% of the depths [m]
i	=	Time increment index [−]
$L_{om\text{-}1,0}$	=	Deep-water wave length based on $T_{m\text{-}1,0}$ [m]
m	=	Exponent [−]
N	=	Total number of increments in overtopping wave [−]
N_w	=	Total number of incident wave in an experiment [−]
n	=	Exponent [−]
P_V	=	Probability of individual overtopping wave exceeding a specified value [−]
$q(t)$	=	Time-varying overtopping discharge per unit dike length [m^3/s per m]
q_c	=	Critical discharge [m^3/s per m]
q_i	=	Best-fit (or predicted) value of instantaneous discharge at time increment, i [m^3/s per m]

(continued on next page)

$\overline{q}_m$	=	Mean of measured instantaneous discharges in an overtopping wave [m^3/s per m]
$q_{m,i}$	=	Measured instantaneous discharge at time increment, i [m^3/s per m]
q_{max}	=	Maximum instantaneous discharge in an overtopping wave [m^3/s per m]
q_{maxT}	=	Theoretical maximum discharge in an overtopping wave [m^3/s per m]
q_{meanT}	=	Theoretical mean discharge in an overtopping wave [m^3/s per m]
q_w	=	Average overtopping discharge [m^3/s per m]
R_c	=	Dike freeboard (crest elevation – still water level) [m]
$R_{u2\%}$	=	Vertical run-up elevation exceeded by 2% of the run-ups [m]
r^2	=	Coefficient of determination [−]
SSE	=	Sum of squared errors [m^3/s per m or m^3/m, depending on usage]
SSR	=	Sum of squared residuals [m^3/s per m or m^3/m, depending on usage]
T_A	=	Time when instantaneous discharge first exceeds critical discharge [s]
T_B	=	Time when instantaneous discharge again equals critical discharge [s]
$T_{m-1,0}$	=	Mean spectral wave period [s]
T_o	=	Duration of individual overtopping wave [s]
T_{oT}	=	Theoretical duration of an overtopping wave [s]
T_p	=	Wave period associated with the spectral peak [s]
t	=	Time [s]
t_{max}	=	Measured time of maximum discharge in an overtopping wave [s]
t_{maxT}	=	Theoretical time of maximum discharge in an overtopping wave [s]
u	=	Overtopping velocity parallel to dike surface [m/s]
$u(t)$	=	Time-varying overtopping velocity parallel to dike surface [m/s]
u_c	=	Critical velocity [m/s]
u_{max}	=	Maximum instantaneous velocity in an overtopping wave [m/s]
$u_{2\%}$	=	Flow velocity at seaward side of dike crest exceeded by 2% of the velocities [m/s]
$V(t)$	=	Time-varying cumulative overtopping volume per unit dike length [m^3/m]
V_E	=	Excess volume per unit dike length in an overtopping wave [m^3/m]
V_i	=	Best-fit (or predicted) value of cumulative wave volume at time increment, i [m^3/m]
$\overline{V}_m$	=	Mean of measured cumulative volume in an overtopping wave [m^3/m]
$V_{m,i}$	=	Measured cumulative wave volume at time increment, i [m^3/m]
V_T	=	Total water volume in an overtopping wave per unit dike length [m^3/m]
W_E	=	Excess flow work per unit dike length in an overtopping wave [m^3/m]
x_c	=	Horizontal dimension on dike crest [m]
Greek symbols		
α	=	Angle of seaward-side dike slope relative to horizontal [rad]

Acknowledgements

The authors are deeply grateful for being allowed access to the comprehensive, high-quality data gathered during the *FlowDike 1* and *FlowDike 2* experiments, funded by the European Community (Hydralab-project HyIII-DHI-5), the German Ministry of Research, and the German Coastal Research Council (03KIS075 and 03KIS076). The data quality and accompanying documentation (Lorke et al., 2009) are a tribute to the *FlowDike* chairman, Dr. Holger Schüttrumpf, and the entire *FlowDike* team. Special thanks to Dr. Jentsje W. van der Meer for providing the *FlowDike* data and assisting during the initial phases of data extraction and data quality assessment. The authors sincerely appreciate the constructive and beneficial review comments and suggestions provided by the reviewers.

Appendix A. Supplementary data

Supplementary data to this article can be found online at http://dx.doi.org/10.1016/j.coastaleng.2016.08.006.

References

Bosman, G., Van der Meer, J.W., Hoffmans, G., Schüttrumpf, H., Verhagen, H.J., 2008. Individual overtopping events at dikes. Proceedings of the 31st International Conference Coastal Engineering. 4. American Society of Civil Engineers, pp. 2944–2956.

Dean, R.G., Rosati, J.D., Walton, T.L., Edge, B.L., 2010. Erosional equivalences of levees: Steady and intermittent wave overtopping. In: Demirbilek (Ed.), Special Issue of Ocean Engineering 37. Elsevier, pp. 104–113.

Hughes, S.A., 2011. Adaptation of the Levee Erosional Equivalence Method for the Hurricane Storm Damage Risk Reduction System (HSDRRS)," ERDC/CHL TR-11-3. U.S. Army Engineer Research and Development Center, Vicksburg, Mississippi.

Hughes, S.A., 2015a. "Hydraulic Parameters of Individual Overtopping Wave Volumes," Technical Report. Engineering Research Center, Colorado State University, Fort Collins, CO (68pp).

Hughes, S.A., 2015b. Hydraulic parameters of overtopping wave volumes," Proceedings of Coastal Structures 2015. American Society of Civil Engineers, New York in press.

Hughes, S.A., Nadal, N.C., 2009. "Laboratory Study of Combined Wave Overtopping and Storm Surge Overflow of a Levee," Coastal Engineering. 56. Elsevier, pp. 244–259 No. 3.

Hughes, S.A., Thornton, C.I., Van der Meer, J.W., Scholl, B.N., 2012. "Improvements in Describing Wave Overtopping Processes," Proceedings of the 33rd International Conference Coastal Engineering. American Society of Civil Engineers Available at: https://journals.tdl.org/icce/index.php/icce/article/download/6684/pdf_659.

Lorke, S., Brüning, A., Bornschein, A., Gilli, S., Krüger, N., Schüttrumpf, H., Pohl, R., Spano, M., Werk, S., 2009. Influence of wind and current on wave run-up and wave overtopping. Hydralab – FlowDike, Report 2009 (100pp).

Lorke, S., Brüning, A., Van der Meer, J., Schüttrumpf, H., Bornschein, A., Gilli, S., Pohl, R., Spano, M., Řiha, J., Werk, S., Schlütter, F., 2010. On the effect of current on wave run-up and wave overtopping. Proceedings of the 32nd International Conference Coastal Engineering, Shanghai, China. American Society of Civil Engineers, New York Available at https://journals.tdl.org/icce/index.php/icce/article/download/1388/pdf_366.

Pullen, T., Allsop, N.W.H., Bruce, T., Kortenhaus, A., Schüttrumpf, H., Van der Meer, J.W., 2007. EurOtop: Wave overtopping of sea defences and related structures: Assessment Manual. Available at: www.overtopping-manual.com.

Schüttrumpf, H., Oumeraci, H., 2005. Layer thicknesses and velocities of wave overtopping flow at seadikes. Coastal Engineering 52. Elsevier, pp. 473–495.

Schüttrumpf, H., Van Gent, M.R., 2003. Wave overtopping at sea dikes. Proceedings of Coastal Structures 2003. American Society of Civil Engineers, pp. 431–443.

Schüttrumpf, H., Möller, J., Oumeraci, H., 2002. Overtopping flow parameters on the inner slope of seadikes. Proceedings of the 28th International Coastal Engineering Conference 2. World Scientific, pp. 2116–2127.

Steendam, G.J., Van der Meer, J.W., Hardeman, B., Van Hoven, A., 2010. Destructive wave overtopping tests on grass covered landward slopes of dikes and transitions to berms. Proceedings of the 32nd International Conference Coastal Engineering. American Society of Civil Engineers Available at https://journals.tdl.org/icce/index.php/icce/article/download/7965/pdf_980.

Thornton, C.I., Hughes, S.A., Scholl, B.N., Youngblood, N., 2014. Estimating grass slope resiliency during wave overtopping: results from full-scale overtopping simulator testing. Proceedings of the 34th International Conference Coastal Engineering. American Society of Civil Engineers Available at: https://journals.tdl.org/icce/index.php/icce/article/download/7523/pdf_78.

Thornton, C.I., Van der Meer, J.W., Scholl, B.N., Hughes, S.A., Abt, S.R., 2011. Testing levee slope resiliency at the new Colorado State University wave overtopping test facility. Proceedings of 6th International Conference on Coastal Structures. World Scientific, Singapore.

Van der Meer, J.W., 2007. Design, Construction, Calibration and Use of the Wave Overtopping Simulator," version 3.3, CUR Project 04i103 Report, INFRAM 108pp.

Van der Meer, J.W., Hardeman, B., Steendam, G.J., Schüttrumpf, H., Verheij, H., 2010. Flow depths and velocities at crest and inner slope of a dike, in theory and with the wave overtopping simulator. Proceedings of the 32nd International Coastal Engineering Conference. American Society of Civil Engineers Available at: https://journals.tdl.org/icce/index.php/icce/article/download/1239/pdf_260.

Van der Meer, J.W., Snijders, W., Regeling, E., 2006. The wave overtopping simulator. Proceedings of the 30th International Coastal Engineering Conference 5. American Society of Civil Engineers, pp. 4654–4666.

Van der Meer, J.W., Steendam, G.J., de Raat, G., Bernardini, P., 2008. Further developments on the wave overtopping simulator. Proceedings of the 31st International Conference Coastal Engineering 4. American Society of Civil Engineers, pp. 2957–2969.

Van der Meer, J.W., Thornton, C., Hughes, S., 2011. Design and operation of the US wave overtopping simulator. Proceedings of 6th International Conference on Coastal Structures. World Scientific, Singapore.

Van Gent, M.R., 2002. Wave overtopping events at dikes. Proceedings of the 28th International Coastal Engineering Conference 2. World Scientific, pp. 2203–2215.